In situ analysis of local strain distribution of amorphous polyrotaxane adhesives constrained by metal substrates

Kazuaki Kato,[1,2,3] Ayumu Takeshima,[1] Kenichiro Ryu,[1] Kohzo Ito,[1] Masanobu Naito,[1,3] Yoshiki Kohmura,[2] and Taiki Hoshino[2,4,5]**

[1]Department of Advanced Materials Science, Graduate School of Frontier Sciences, The University of Tokyo, 5-1-5 Kashiwanoha, Kashiwa, Chiba 277-8561, Japan

[2] RIKEN SPring-8 Center, 1-1-1, Kouto, Sayo-cho, Sayo-gun, Hyogo 679-5148, Japan

[3] Research Center for Macromolecules and Biomaterials, National Institute for Materials Science, Tsukuba, Ibaraki 305-0047, Japan

[4] International Center for Synchrotron Radiation Innovation Smart, Tohoku University, Sendai 980-8577, Japan

[5] Institute of Multidisciplinary Research for Advanced Materials, Tohoku University, Aoba-ku, Sendai 980-8577, Japan

KEYWORDS: adhesion, buried interface, X-ray nanobeam diffraction, strain-distribution analysis, deformation and fracture processes, polyrotaxane, strain delocalization.

ABSTRACT

In situ structural analysis under loads of amorphous adhesives buried between metal substrates was conducted using synchrotron X-ray nanobeam diffraction and an embedded local strain probe. Thermoplastic resins composed of polyrotaxanes, featuring bulky cyclic molecules threaded with a linear polymer, were sandwiched between stainless-steel substrates, with diffraction data attributed to the correlation distance between their cyclic components being collected. The nanobeam was irradiated parallel to the substrates and scanned while distances from the substrate were changed to obtain depth profiles of correlation distance. Then, tensile loads were applied stepwise on the sandwiched sample to reveal local strain distributions of the resins under different loads. Different strain distributions and their changes with loads were observed in resins with different adhesive strengths. The sample with strong adhesion showed pronounced strain localization near the interface between resin and substrate, whereas the weak sample displayed moderate strain further from the interface, with a negligible strain near the interface. When the load increased, localized strain saturation occurred, followed by strain propagation into adjacent areas, indicative of a typical strain delocalization process associated with strain hardening near highly constrained interface by substrates. This analysis elucidated the deformation and fracture processes of buried polymers, offering insight into those adhesive strength differences phenomenologically. This in situ analysis of local strain distribution contributes to comprehending adhesion mechanisms required for advancing multimaterialization technology and holds applicability to materials with buried interfaces, such as nanocomposites.

INTRODUCTION

The growth of fundamental sciences of adhesion is required for the development of multimaterialization technology, contributing to environmental impact reduction by e.g., reducing the weight of transportation equipment. Adhesives, usually organic resins, are useful for bonding inorganic structural materials, such as steel and aluminum alloys. To design adhesives rationally, a comprehensive understanding of the deformation and fracture process of polymers not only in the bulk state but also under the constraints imposed by inorganic substrates is indispensable. However, analyzing adhesive structures buried between substrates, which shield X-ray and electron beams, presents considerable challenges. These buried interfaces can be exposed to the surface via ultralow-angle microtomy,[1] enabling the application of conventional surface analysis methods to reveal structures at certain moments during the fracture process.[2,3,4] Conversely, for nondestructive analysis, recent advancements in interface-sensitive analyses have been notable. Sum frequency generation vibrational spectroscopy, for instance, has revealed specific molecular orientations of buried polymers at the surface of transparent inorganic substrates.[5] The distinct characteristics of surface (interface) molecules are intricately linked with adhesion and are pivotal considerations in adhesive designs.[6] Additionally, neutron and X-ray reflectivity offers a high-depth resolution, revealing composition differences of buried polymers near the interface.[7]

Synchrotron X-ray diffraction is a powerful tool for multiscale structural analysis, offering the capability for in situ analysis under load conditions. Recent discussions have delved into the deformation and fracture process of bulk polymers, often subjected to uniaxial tensile load, leveraging parameters such as crystal lattice strains, crystal orientations, and nanovoid formations.[8,9,10] Another advantage of synchrotron X-ray diffraction is local structure analysis using microbeams. For instance, the crystal orientation of polyamide 6 near its interface with a

carbon fiber was analyzed by transmitting a microbeam parallel to the interface.[11] The obtained orientation profile indicated the presence of a specific layer with several micrometers in thickness, where crystalline polymers were oriented along the fiber direction. These long-range effects of interface constraints extend to amorphous polymers as well,[12,13] with the thickness of the constrained area hypothesized to influence adhesion strength between polymers and substrates considerably.[14] Thus, in situ structural distribution analyses around adhesion interfaces under load conditions are expected to reveal the deformation and fracture processes directly connected to adhesion properties between polymers and inorganic materials.

A new series of biobased amorphous polymers featuring cyclic oligosaccharides threaded with a linear polymer, termed polyrotaxanes (inset of Figure 1a), were utilized to improve the toughness of epoxy resins[15] and their adhesion strengths on metal substrates.[16] Recently, an in situ X-ray diffraction study of bulk polyrotaxane resins under uniaxial tension revealed a unique toughening mechanism related to strain-induced structural transformation.[17] Although polyrotaxanes are glassy and amorphous, they yield various structural information via X-ray diffraction. The cyclic molecules, cyclodextrins (CDs), are the major component of the polyrotaxane resins with a higher electron density compared to the polymer component and are distributed homogeneously in the resins, resulting in the observation of broad diffraction (amorphous halo) reflecting the correlation distance between CDs, d_{CD} (Figure 1b).[18] In addition, the orientation of CDs in the resins appears as anisotropy in another amorphous halo attributed to the correlation distance between glycosidic oxygen atoms of CD.[19] The diffraction with d_{CD} serves as a probe for local strain in the resins, a crucial parameter alongside stress in understanding materials deformation and fracture processes. Herein, we report an in situ strain-distribution analysis of buried interfaces between polyrotaxane resins and metal substrates using a focused synchrotron X-ray nanobeam that enters parallel to the

substrate surface, as shown in Figure 1a. The depth profile of strain and its variation with load were compared in two polyrotaxanes on the same metal substrate with different adhesion strengths, **nB** and **iB**, with low and high strengths, respectively, to discuss the correlation between their adhesion strengths and deformation processes.

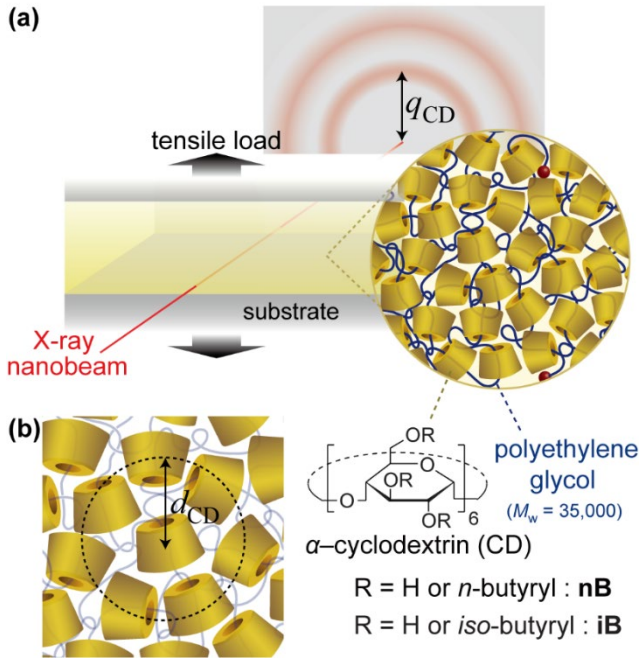

Figure 1. (a) Schematic illustrations of the measurement setup and the structures of polyrotaxane resins constrained between two substrates for this study. (b) Correlation distance between CDs, which are the major components distributed homogeneously with higher electron densities compared to the threading polymers. The distance, d_{CD}, appears as an amorphous halo at the scattering vector, q_{CD}.

EXPERIMENTAL METHODS

Sample preparation. Two types of 304 stainless-steel substrates were bonded together using thermoplastic polyrotaxanes, as shown in Figure 2a. Two types of polyrotaxanes with different acyl groups modified on their ring components were employed: one is *n*-butylated polyrotaxane

(**nB**), and the other is isobutylated polyrotaxane (**iB**). The synthesis of these polyrotaxanes followed literature procedures,[20] with detailed procedures and characterization results described in Supporting Information (Figure S1). Initially, the upper substrate was attached to the polyrotaxane via melt-press molding in a metal mold, as shown in Figure 2b. The melt-press conditions were at 443 K under 10 MPa for 10 min. Then, it was placed atop the pre-polished lower substrate, and a small amount of acetone (<2 μL) was injected into the adhesion interface. After drying under atmospheric conditions, the sample specimen was annealed at 393 K (for **nB**) or 413 K (for **iB**), which were slightly higher than their respective glass transition temperatures for 12 h under vacuum.

Structural analysis under tensile loads. Synchrotron X-ray diffraction measurements were performed at SPring-8 BL29XUL (Hyogo, Japan)[21] using incident X-ray beam energy of 15 keV. The experimental setup for the synchrotron X-ray diffraction measurement is shown in Figure 2c. Synchrotron X-rays were focused using a Pt-coated elliptical-cylinder mirror, with the beam size measured via the conventional wire scan method. As shown in Figure 2d, the beam size perpendicular to the substrate was determined at 789 nm at full width at half maximum, while the horizontal beam size was ~30 μm. The incident X-ray nanobeam was directed parallel to the interface between the lower substrate and polyrotaxane, as shown in Figure 2e. To avoid the influence of sample shape, the X-ray nanobeam was irradiated near the center of the interface along the x-axis direction rather than near the sample edges. The sample was fixed on a movable stage, and the upper substrate with a hole was pulled up to apply a tensile load. By moving the stage, X-rays were scanned from the lower substrate to the polyrotaxane to capture scattering images at different heights from the interface, denoted as h. The exposure time and data acquisition time for each irradiation point were 10 and 12 s, respectively. Diffraction images were collected

using an EIGERX1M (Dectris) detector with a sample-to-detector distance of 253 mm. A representative 2D diffraction image is shown in Figure 2f. The diffraction perpendicular to the substrate, aligned with the tensile direction within ±10 °, was sector averaged to obtain the profile of diffraction intensity depending on the scattering vector, q. A representative scattering profile of polyrotaxane resins is shown in Figure 2g. Two strong but broad diffractions were detected near 5 and 15 nm^{-1}, corresponding to the correlation distance between rings (Figure 1b) and between glycosidic oxygen atoms in the ring, respectively. The q value of the halo near 5 nm^{-1}, denoted as q^1_{peak}, was tracked to analyze the local strain, as explained below.

This X-ray diffraction analysis was also performed under tensile load by pulling up the upper substrate using a lifting device connected to a load cell. Tensile loads were applied stepwise to facilitate the abovementioned X-ray scanning under different loads. The lifting device operated at a speed of 1 μm/s. Upon each predetermined load, immediately after the lifting device stopped, a rapid load relaxation was observed. X-ray scanning started after the load value became constant, confirmed through load measurements taken before and after scanning. The magnitude of load relaxation tended to increase with increasing applied maximum load (see Table S1 in the Supporting Information). The load values stated in this study are the applied maximum loads, which were instantaneously recorded before the relaxations occurred.

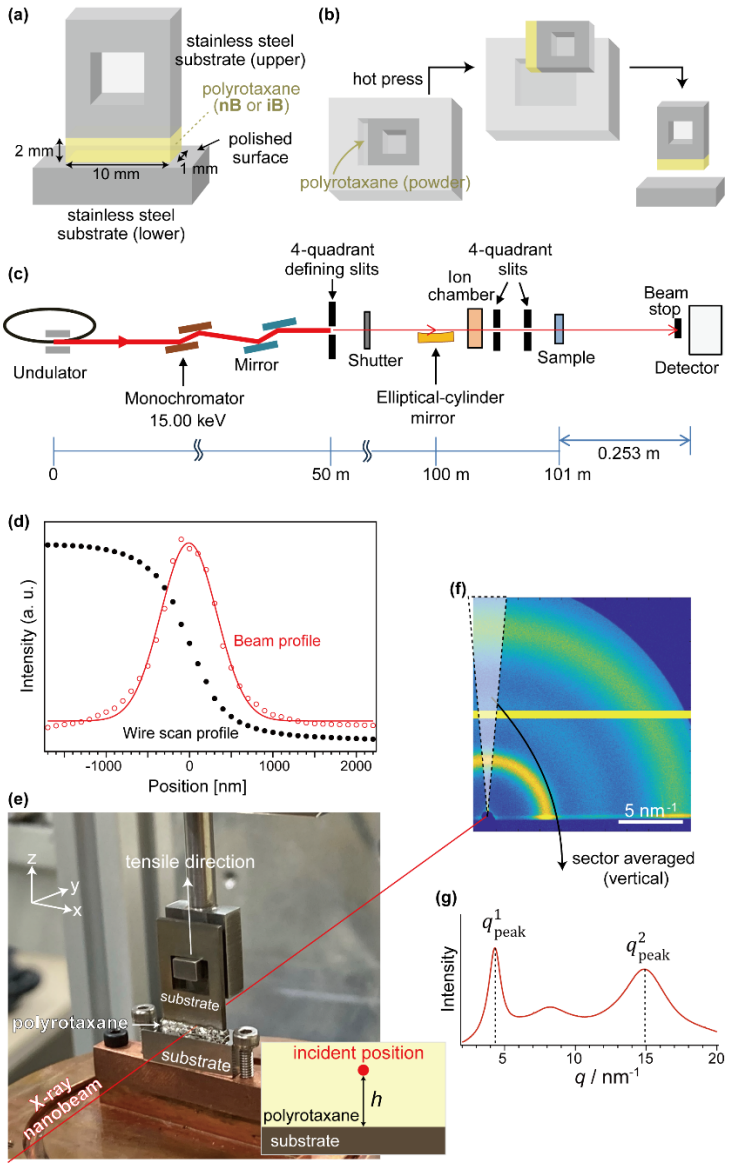

Figure 2. (a) Schematic illustration of a sample specimen adhered on stainless-steel substrates using polyrotaxane and (b) its preparation scheme. (c) Schematic drawing of the experimental set up. X-rays, cut by four-quadrant defining slits placed 50 m from the undulator source, were vertically focused on the sample position using the elliptical-cylinder mirror. (d) Result of beam-size measurement via wire-scanning method. (e) Set up around the sample for measurement under tensile load at different heights from the interface between the substrate and polyrotaxane, *h*. (f) A representative 2D diffraction pattern and (g) a sector-averaged 1D profile perpendicular to the interface.

RESULTS AND DISCUSSION

A considerable difference in adhesion strength was observed between **nB** and **iB**. Figure 3 shows the results of the adhesion strength test conducted under a constant tensile displacement. The same test was also conducted alongside the structural analysis, except for a stepwise displacement application on the sample specimens. Although both bulk polyrotaxanes exhibit similar Young's moduli (0.9 and 1.0 GPa for **nB** and **iB**, respectively), the adhesion strength of **iB** was notably higher than that of **nB**. However, under a conventional lap-shear test, higher adhesion strength was observed in **nB** compared to **iB** (Figure S2). Notably, the deformation mode employed in this study involves strong dilatational stress under strong strain constraints imposed by substrates, unlike the lap-shear test, which does not involve volume change. We only have a speculation that these two materials might have different bulk modulus and are subject to different stress fields, although it is not the main concern of this report.

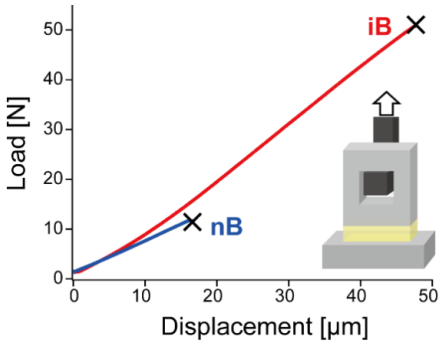

Adhesive	Breaking Load [N]
iB	41 ± 9
nB	25 ± 11

Figure 3. Representative load–displacement curves and averaged breaking loads (n = 4) obtained from steady tensile tests of sample specimens shown in Figure 2a. The crosshead speed remained constant at 1 μm/s.

The X-ray nanobeam was irradiated onto samples of **nB** and **iB**, matching the shape of those used in the abovementioned adhesion strength tests. The broad diffraction peak observed near q =

4.5 nm^{-1}, characteristic of polyrotaxanes in the melt and glass states, is attributed to the correlation distance between CDs.[12] CDs, being the major component of polyrotaxane, are homogeneously dispersed throughout the material, possessing higher electron density than polyethylene glycol. Consequently, this diffraction has been utilized as a probe for local strain of amorphous polyrotaxane resins.[11,12] The correlation distance between CDs, d_{CD}, was obtained from the peak q value, q^1_{peak}, as follows:

$$d_{CD} = 2\pi/q^1_{peak}. \quad (1)$$

Figure 4a shows representative wide-angle X-ray diffraction profiles at different h for an **nB** sample under no load. The position of Peak 1 shifts to low q with increasing h, indicating that the inter-CD distance was small in the vicinity of the interface and increased with distance from it. The h dependence of d_{CD}, obtained through Eq. 1, is illustrated in Figure 4b. This diffraction measurement was finely conducted near the interface (every 0.3 μm when $h \leq 12$ μm) and sparsely further from the interface (every 3 μm when $h > 12$ μm). Additionally, another peak observed near $q = 15$ nm^{-1} (peak 2) is attributed to an intramolecular atomic distance of CD.[19] The q value, q^2_{peak}, represents the correlation distance between six glycosidic oxygen atoms in a single CD molecule. No peak shift was observed at different h, confirming that the molecular structure of CD was maintained.

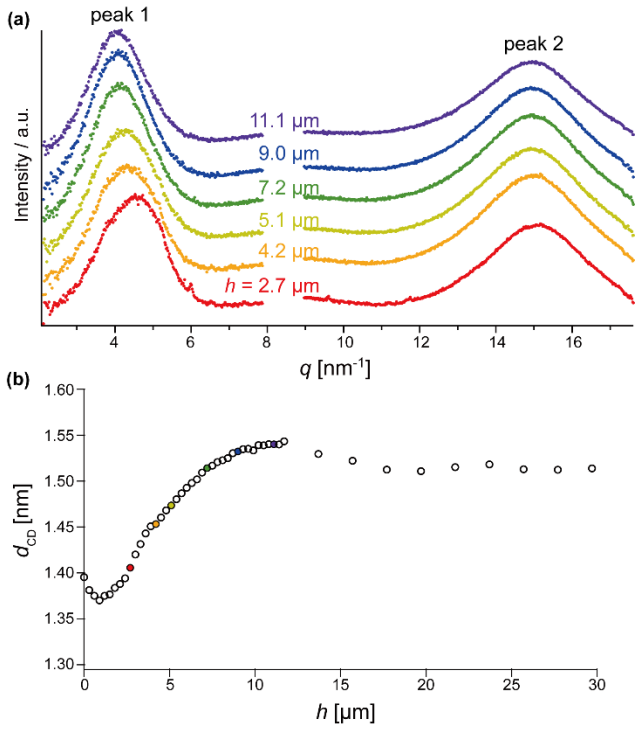

Figure 4. (a) Representative partial wide-angle X-ray diffraction profiles near q^1_{peak} of **nB** before loading (0 N), showcasing different distances from the substrate, h, and (b) the dependence of correlation distance between CDs, d_{CD}, on h.

To explore the changes in the h-dependent profile of d_{CD} in the **nB** sample under tension, scanning was conducted under various loading conditions. During the measurements under load, the crosshead was displaced in the tensile direction, and after reaching the target load, X-ray scanning measurements were performed following a brief waiting period for the load to become constant. Figure 5a shows the h-dependent profiles of d_{CD} under different loads of 0, 8, and 18 N, acquired before fracture (these data were obtained from a different **nB** sample than that shown in Figure 4a). Under 0 N, the d_{CD} of **nB** far from the interface (h > 100 μm) was 1.47–1.50 nm, nearly identical to that of a freestanding bulk sample (unconstrained by substrates) of **nB**. Conversely, d_{CD} near the substrate, particularly at 10 < h < 100 μm, showed slightly high values. It is possibly

associated with the remarkably suppressed dynamics of polymers adsorbed on the substrate that may influence the annealing state of adhesives.[13,22] Under tensile load, d_{CD} values of **nB** increased at almost all h, indicating a reasonable change in the distance between CDs as they diverge in the tensile direction. However, this change appeared to be more moderate near the interface compared to farther from the interface. It suggests that the local strain near the interface is relatively small. Engineering tensile strain is generally defined as the quotient of increment of length between gauge points divided by the initial length. Because the CDs dispersed in this material homogeneously in the beginning, the distance between CDs work as microscopic gauge. Here, we define the local tensile strain of polyrotaxane adhesives, ε_{CD}, as follows:

$$\varepsilon_{CD} = \frac{d_{CD} - d_{CD,0}}{d_{CD,0}}, \quad (2)$$

where d_{CD} and $d_{CD,0}$ are the correlation distance between CDs after and before loading, respectively. The obtained ε_{CD} values, depending on h, are depicted in Figure 5b. Local strain increased at almost all h as the load escalated from 8 to 18 N. Notably, the area near the interface at h < 20 μm exhibited minimal strain, even under 18 N. Local strain gradually increased with distance from the substrate, slightly exceeding a strain of 0.02 farther from the interface. This strain, indicated by the dashed line in the graph, corresponds to the macroscopic strain under 18 N estimated as the tensile force over the Young's modulus over the cross-sectional area. The maximum local strain remains below 0.05, indicating no pronounced strain localization in the case of **nB**.

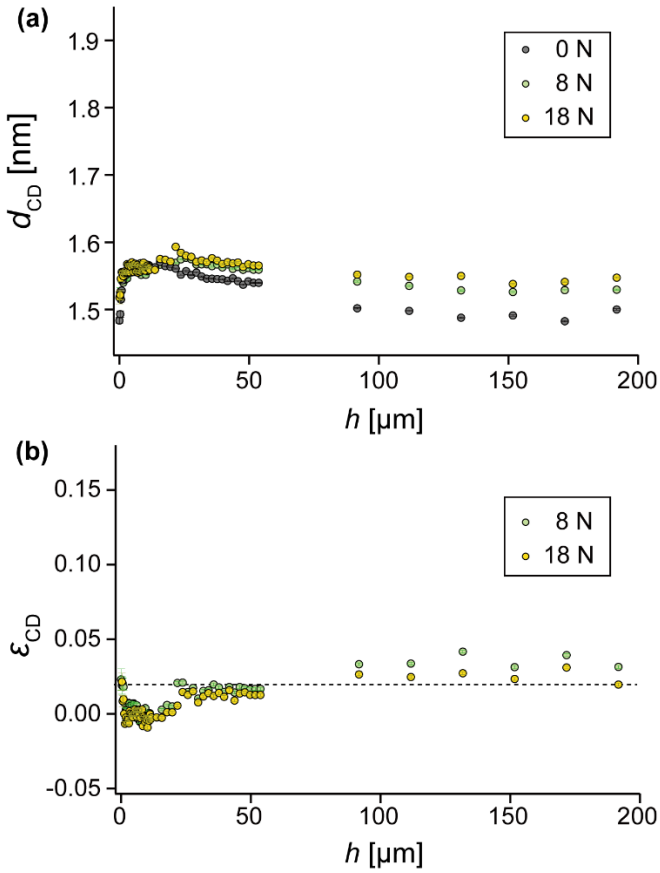

Figure 5. Dependence on the distance from the substrate, h, of (a) the correlation distance between CDs and (b) the local strain under different tensile loads on **nB**. The dashed line represents the calculated macroscopic strain under 18 N.

In contrast, the strain was strongly localized near the interface in the case of **iB**, exhibiting enhanced adhesion strength sufficient for structural analysis until 22 N. Before loading, as shown in Figure 6a, d_{CD} at $h > 50$ μm remained constant, almost identical to that of a freestanding bulk **iB**. Approaching the interface, d_{CD} increased and then sharply decreased toward the surface. This distribution of d_{CD} in **iB** before loading resembles that of **nB**. However, upon application of tensile stress on **iB** samples, d_{CD} dramatically increased in the region near $h = 10$ μm. Using Eq. 2, the d_{CD} values of **iB** were converted into local strains, and their h dependence is plotted in Figure 6b. The

strain indicated by the dashed line in the graph corresponds to the macroscopically averaged strain of **iB** under 18 N as well. Near the interface at $h < 30$ μm, the extremely high strain was localized even under 18 N in **iB**. Conversely, a negligible strain, considerably lower than the averaged strain, was observed at $h > 50$ μm even under 22 N. Considerably high strains were localized at a small area near the interface for **iB**, marking a stark contrast to the strain distributions observed in **nB**.

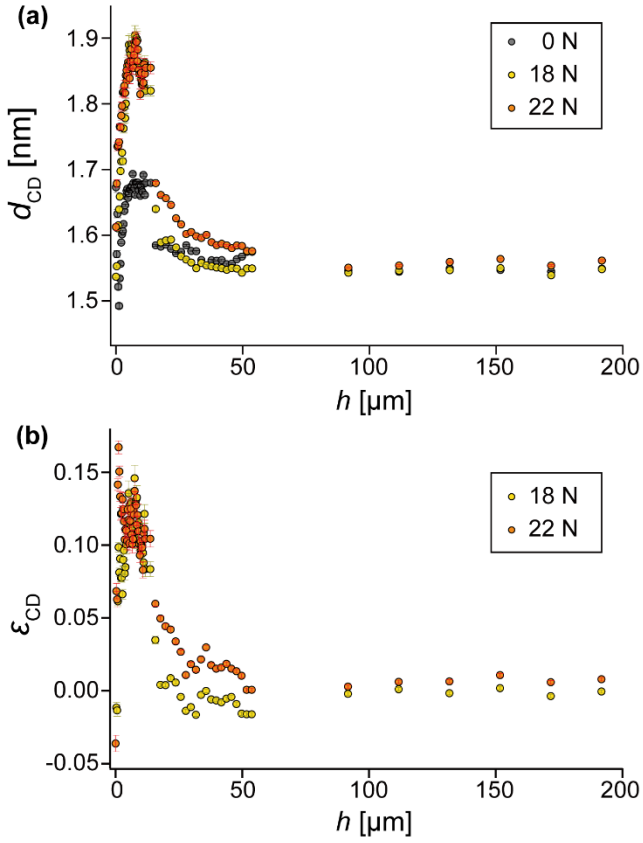

Figure 6. Dependence on distance from the substrate of (a) correlation distance between CDs and (b) local strain under different stresses of **iB**. The dashed line represents the calculated macroscopic strain under 18 N.

Strain localization usually leads to macroscopic fracture originating from the strain-localized area. Although strain localization can be reduced using soft materials, the adhesion strength may

be compromised. Moreover, adhesives are subjected to strong strain constraints between substrates, making it unrealistic to entirely avoid strain localization. However, the strain localization observed in **iB** resulted in a rather stronger adhesion strength compared to **nB**, despite having a similar Young's modulus to **iB**. Figure 7a shows an enlarged view of the strain-localized area of **iB** shown in Figure 6b. Under a load of 18 N, the highest local strain in **iB** occurred near h = 7 μm, with almost no strain observed at h > 15 μm. However, increasing the load to 22 N did not further increase the maximum localized strain. The highest strain near h = 7 μm (~0.13) remained unchanged with the increased load. Instead, strain in the adjacent parts (indicated by arrows in the graph) considerably increased. The strain began to appear at h > 15 μm with increasing load where no strain was observed under 18 N, while very high strain emerged in the area closest to the interface (h < 5 μm). This result indicates a delocalization process of strain in **iB**, as schematically shown in Figure 7b. Strain localization directly leads to macroscopic fracture of materials as long as no strain hardening occurs in the strain-localized area.[23,24,25] In this case, the adhesive would typically fracture near h = 7 μm. However, the local strain in this area reached saturation at ε_{CD} of ~0.13. This strain is close to the yielding strain of freestanding polyrotaxane films under uniaxial tension, where yielding entails a unique structural transformation that hardens the initially strain-localized area, facilitating strain delocalization.[14] Probably because of the same strain-hardening mechanism, the initially strain-localized area near h = 7 μm hardened sufficiently to delocalize the strain to adjacent areas of **iB**. Although multiscale structural analyses and simulation studies are necessary to delve into generalized structure–property relationships, the elucidation of strain distribution and its progress with increasing load allows for a phenomenological explanation of the different deformation and fracture processes associated with varying adhesion strengths.

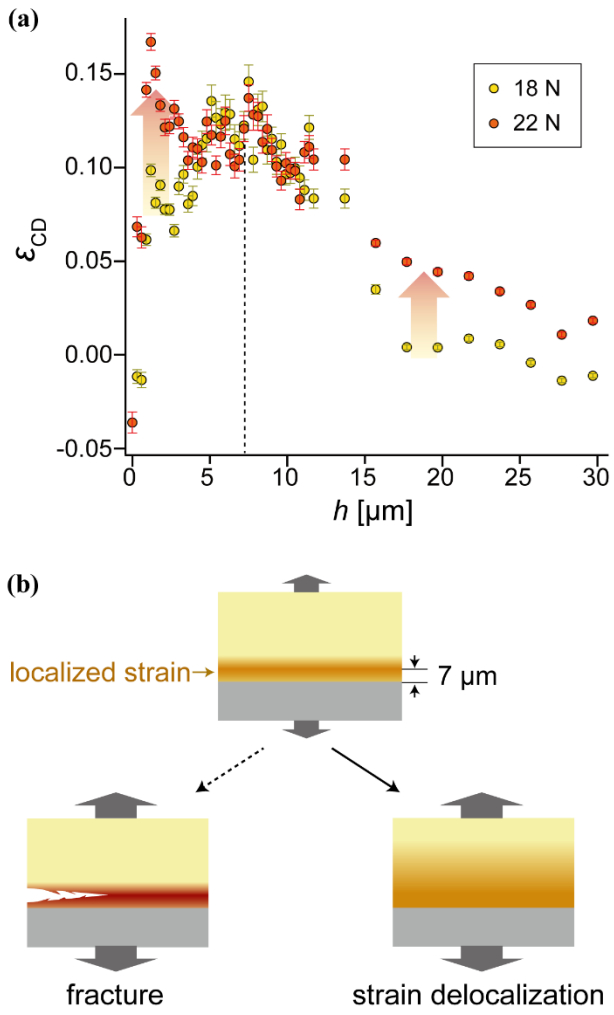

Figure 7. (a) Evolution of local strain ε_{CD} distribution near the interface of **iB** with increasing tensile load (magnified graph of Figure 6b). Colored arrows indicate areas with profound changes in strain as the load increased from 18 to 22 N. (b) Schematic illustration of strain localization near the interface, which could lead to fracture and the subsequent delocalization of strain owing to strain hardening.

CONCLUSION

Herein, we demonstrated an analysis of the local strain distribution of amorphous polyrotaxane adhesive at buried interfaces between stainless-steel substrates using synchrotron X-ray nanobeam diffractions under tensile loads. The main component molecules of polyrotaxane worked as strain probes to reveal depth-dependent strain profiles and their changes under increased loads. Two different strain-distribution profiles emerged in the two different polyrotaxanes examined: one with high adhesion strength showed strong strain localization near the interface, whereas the other showed minimal strain near the interface but distributed small strains over a wide range of depth. The observed changes in strain distribution with increased loads indicate a process of strain delocalization near the interface, likely contributing to enhanced adhesion of polyrotaxane resins and metal substrates. Through our local strain-distribution analysis under loads, the processes of deformation and strain delocalization within the buried polymers were revealed, allowing for a phenomenological explanation of the differences in adhesion strength. Unlike digital image correlation (DIC) or micro-DIC, which require a random patterning on the surface of materials,[26,27] X-ray diffraction mainly captures those inner structures, where strain is strongly constrained, leading to distinct deformation processes compared to the surface. In addition, the resolution of this analysis was limited only by the X-ray beam size, which has recently been achievable at several nanometers.[28] Moreover, simultaneous detection of small-angle scattering is technically possible, enabling elucidation of mesoscale fracture processes, such as nanovoid formations and crazing.[29] These multiscale fine structural mappings, facilitated this reported method, not only elucidating the behavior of polyrotaxanes at interfaces, strengthening various interfaces with inorganic materials, but also contributing to the progress of fundamental adhesion science, facilitating rational adhesive designs.

ASSOCIATED CONTENT

Supporting Information

The Supporting Information is available free of charge on the ACS Publications website.

Synthesis and characterization of polyrotaxane resins, result of X-ray beam-size measurement, and depth profiles of X-ray diffraction. (PDF)

AUTHOR INFORMATION

Corresponding Author

Kazuaki Kato

*Corresponding; E-mail: kkato@edu.k.u-tokyo.ac.jp

Taiki Hoshino

*Corresponding; E-mail: taiki.hoshino.c7@tohoku.ac.jp

Author Contributions

The manuscript was written through contributions of all authors. All authors have given approval to the final version of the manuscript.

Funding Sources

This work was supported by a JSPS KAKENHI grant (20H02794).

ACKNOWLEDGMENT

We appreciate JASRI/SPring-8 optics team members of beamline division for designing the ellipsoidal mirror. We appreciate also Materials Fabrication and Analysis Platform of Research

Network and Facility Services Division in National Institute for Materials Science Japan, particularly Koji Nakazato for painstaking surface polishing of stainless-steel substrates and Chiho Togashi for fabrication of the special fixtures for measurements.

ABBREVIATIONS

CD, Cyclodextrin; DIC, Digital image correlation

REFERENCES

1. S. J. Hinder, C. Lowe, J. T. Maxted, and J. F. Watts, The Morphology and Topography of Polymer Surfaces and Interfaces Exposed by Ultra-Low-Angle Microtomy, *J. Mater. Sci.* **2005**, *40*, 285–293.

2. N. Baden, Novel Method for High-Spatial-Resolution Chemical Analysis of Buried Polymer-Metal Interface: Atomic Force Microscopy-Infrared (AFM-IR) Spectroscopy with Low-Angle Microtomy, *Appl. Spectrosc.* **2021**, *75*, 901–910.

3. S. Morsch, Y. Liu, M. Malanin, P. Formanek, K. Eichhorn, Exploring Whether a Buried Nanoscale Interphase Exists Within Epoxy–Amine Coatings: Implications for Adhesion, Fracture Toughness, and Corrosion Resistance, *ACS Appl. Nano Mater.* **2019**, *2*, 2494–2502.

4. J. Sang, H. Hirahara, S. Aisawa, Z. Kang, and K. Mori, Direct Bonding of Polypropylene to Aluminum Using Molecular Connection and the Interface Nanoscale Properties, *ACS Appl. Polym. Mater.* **2019**, *1*, 2450–2459.

5. H. Tsuruta, Y. Fujii, N. Kai, H. Kataoka, T. Ishizone, M. Doi, H. Morita, and K. Tanaka, Local Conformation and Relaxation of Polystyrene at Substrate Interface, *Macromolecules* **2012**, *45*, 4643–4649.

6. B. P. Lee, P. B. Messersmith, J. N. Israelachvili, J. H. Waite, Mussel-Inspired Adhesives and Coatings, *Annu. Rev. Mater. Res.* **2011**, *41*, 99–132.

7. K. Stoev and K. Sakurai, Recent Progresses in Nanometer Scale Analysis of Buried Layers and Interfaces in Thin Films by X-rays and Neutrons, *Anal. Sci.* **2020**, *36*, 901–922.

8. A. Nogales, B. S. Hsiao, R. H. Somani, S. Srinivas, A. H. Tsou, F. J. Balta-Calleja, and T. A. Ezquerra, Shear-Induced Crystallization of Isotactic Polypropylene with Different Molecular Weight Distributions: In Situ Small- and Wide-Angle X-ray Scattering Studies, *Polymer* **2001**, 42, 5247–5256.

9. Y. Ogino, H. Fukushima, N. Takahashi, G. Matsuba, K. Nishida, and T. Kanaya, Crystallization of Isotactic Polypropylene Under Shear Flow Observed in a Wide Spatial Scale, *Macromolecules* **2006**, *39*, 7617–7625.

10. G. Stoclet, J. M. Lefebvre, B. Yeniad, G. Gobius du Sart, and S. de Vos, On the Strain-Induced Structural Evolution of Poly(Ethylene-2,5-Furanoate) upon Uniaxial Stretching: An In-Situ SAXS-WAXS Study, *Polymer* **2018**, *134*, 227–241.

11. D. Kobayashi, Y. T. Hsieh, and A. Takahara, Interphase Structure of Carbon Fiber Reinforced Polyamide 6 Revealed by Microbeam X-ray Diffraction with Synchrotron Radiation, *Polymer* **2016**, *89*, 154–158.

12 D. N. Nieto Simavilla, W. Huang, C. Housmans, M. Sferrazza, and S. Napolitano, Taming the Strength of Interfacial Interactions via Nanoconfinement, *ACS Cent. Sci.* **2018**, *4*, 755–759.

13. W. Ren, X. Wang, J. Shi, J. Xu, H. Taneda, N. L. Yamada, D. Kawaguchi, K. Tanaka, and X. Wang, The Role of the Molecular Weight of the Adsorbed Layer on a Substrate in the Suppressed Dynamics of Supported Thin Polystyrene Films, *Soft Matter* **2022**, *18*, 1997–2005.

14. T. Matsumoto, Y. Shimizu, and T. Nishino, Analyses of the Adhesion Interphase of Isotactic Polypropylene Using Hot-Melt Polyolefin Adhesives, *Macromolecules* **2021**, *54*, 7226–7233.

15. X. S. Wang, H. K. Kim, Y. Fujita, A. Sudo, H. Nishida, and T. Endo, Relaxation and Reinforcing Effects of Polyrotaxane in an Epoxy Resin Matrix, *Macromolecules* **2006**, *39*, 1046–1052.

16. S. Pruksawan, S. Samitsu, H. Yokoyama, and M. Naito, Homogeneously Dispersed Polyrotaxane in Epoxy Adhesive and Its Improvement in the Fracture Toughness, *Macromolecules* **2019**, *52*, 2464–2475.

17. K. Kato, K. Ito, and T. Hoshino, Fracture Process of Mechanically Interlocked Ductile Glass Under Uniaxial Tension, *Macromolecules* **2023**, *56*, 7358–7365.

18. K. Kato, K. Nemoto, K. Mayumi, H. Yokoyama, and K. Ito, Ductile Glass of Polyrotaxane Toughened by Stretch-Induced Intramolecular Phase Separation, *ACS Appl. Mater. Interfaces* **2017**, *9*, 32436–32440.

19. K. Kato, K. Ito, and T. Hoshino, Anisotropic Amorphous X-ray Diffraction Attributed to the Orientation of Cyclodextrin, *J. Phys. Chem. Lett.* **2020**, *11*, 6201–6205.

20. K. Kato, M. Taniguchi, and K. Ito, Tough Glass with Mechanical Bonding Network Anchored by High-Mobility Polymers, *Macromolecules* **2023**, *56*, 1810–1817.

21. K. Tamasaku, Y. Tanaka, M. Yabashi, H. Yamazaki, N. Kawamura, M. Suzuki, and T. Ishikawa, SPring-8 RIKEN Beamline III for Coherent X-ray Optics, *Nucl. Instrum. Methods Phys. Res. Sect. A* **2001**, *467–468*, 686–689.

22. N. G. Perez-de-Eulate, M. Sferrazza, D. Cangialosi, and S. Napolitano, Irreversible Adsorption Erases the Free Surface Effect on the Tg of Supported Films of Poly(4-Tert-Butylstyrene), *ACS Macro Lett.* **2017**, *6*, 354–358.

23. Z. Li, S. Zhao, R. O. Ritchie, and M. A. Meyers, Mechanical Properties of High-Entropy Alloys with Emphasis on Face-Centered Cubic Alloys, *Prog. Mater. Sci.* **2019**, *102*, 296–345.

24. C. C. Hung, S. El-Tawil, and S. H. Chao, A Review of Developments and Challenges for UHPC in Structural Engineering: Behavior, Analysis, and Design, *J. Struct. Eng.* **2021**, *147*, 03121001.

25. J. Rottler, Fracture in Glassy Polymers: A Molecular Modeling Perspective, *J. Phys. Condens. Matter* **2009**, *21*, 463101.

26. F. Grytten, H. Daiyan, M. Polanco-Loria, and S. Dumoulin, Use of Digital Image Correlation to Measure Large-Strain Tensile Properties of Ductile Thermoplastics, *Polym. Test.* **2009**, *28*, 653–660.

27. T. I. Lee, W. Jo, W. Kim, J. H. Kim, K. W. Paik, and T. S. Kim, Direct Visualization of Cross-Sectional Strain Distribution in Flexible Devices, *ACS Appl. Mater. Interfaces* **2019**, *11*, 13416–13422.

28. H. Mimura, S. Handa, T. Kimura, H. Yumoto, D. Yamakawa, H. Yokoyama, S. Matsuyama, K. Inagaki, K. Yamamura, Y. Sano et al, Breaking the 10 nm Barrier in Hard-X-ray Focusing, *Nature Phys.* **2010**, *6*, 122–125.

29. H. R. Brown and E. J. Kramer, Craze Microstructure from Small-Angle X-ray Scattering (SAXS), *J. Macromol.* **1981**, *19*, 487–522.

TOC Graphic

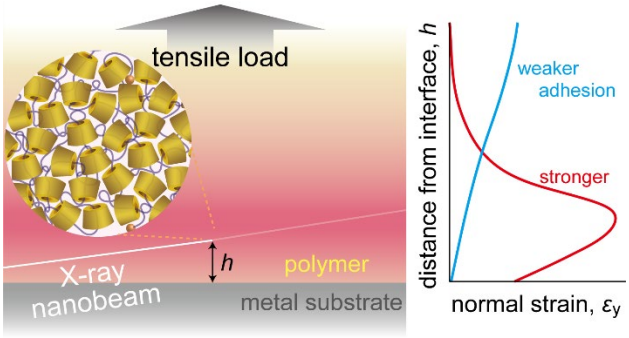
tensile load
X-ray
nanobeam
h
polymer
metal substrate
distance from interface, h
weaker
adhesion
stronger
normal strain, ε_y